Lunar Laser Ranging from Low Earth Orbit

Space Systems
Design Laboratory

AE 8900 MS Special Problems Report
Space Systems Design Lab (SSDL)
Guggenheim School of Aerospace Engineering
Georgia Institute of Technology
Atlanta, GA

Author:
Brandon R. Henley

Advisor:
Prof. Brian C. Gunter

August 1, 2019

Lunar Laser Ranging from Low Earth Orbit

Brian C. Gunter,[1] and Brandon R. Henley[2]
Georgia Institute of Technology, Atlanta, Georgia, 30332, United States of America

Lunar laser ranging (LLR) is an important tool for understanding the physical laws that shape the universe. To date, LLR has only been conducted from Earth-based ground stations, which are subject to the complex dynamics of the solid Earth. In addition, ground-based laser pulses are subject to significant interference as they pass through the atmosphere. In an effort to improve both the precision and frequency of LLR measurements, this paper explores the potential of placing a formation of two small satellites in Low Earth Orbit with the capability of conducting LLR. Such a system would avoid many of the modeling requirements and corrections required for ground stations and would be capable of acquiring more measurements, at equal or higher quality, thereby improving the accuracy of the Earth-Moon distance estimates. This paper attempts to show that such a system is feasible and worth further exploration by the lunar laser ranging community.

I.   Introduction

A. Lunar Laser Ranging Basics

LUNAR laser ranging (LLR) is the process of determining the distance between the Earth and Moon in order to characterize, describe, and understand the orbit of the Moon with respect to the Earth. This is achieved by pointing a laser beam, traditionally ground-based, at the Moon and measuring the time-of-flight (TOF) of the photons in a short pulse of the laser via precise timing electronics and photon detectors. The distance the photons travel is converted from the TOF via the speed of light. LLR pulses are typically measured in terms of their temporal width and are often on the order of hundreds of picoseconds [1] or single nanoseconds. Multiple pulses in rapid succession are often used for statistically increasing the precision of the measurements [1] in concert with calibration, modeling of

---

[1] Assistant Professor, Daniel Guggenheim School of Aerospace Engineering, and AIAA Member Grade.
[2] Graduate Student, Daniel Guggenheim School of Aerospace Engineering.

ground dynamics (e.g. tidal effects and atmospheric pressure loading) and atmospheric turbulence, and data processing. Currently, the Apache Point Observatory Lunar Laser-Ranging Operation (APOLLO) is the LLR station demonstrating the best performance [1] – it maintains a root-mean-square uncertainty (RMS) of less than 3 mm in its ranging measurements, but the data must be fed into an LLR model that accounts for various effects on timing and displacement [1]. The best model as of now, made by the Jet Propulsion Laboratory (JPL) [1], offers an RMS of about 2 cm, and thus the APOLLO measurement uncertainty is superseded by that of the LLR model, which includes it. Thus, the lunar distance is currently determined with certainty to the centimeter level, even though the capability of millimeter level measurement exists.

B. Science Objectives

The fundamental objective of LLR is to precisely determine the lunar distance with respect to the Earth. Currently, the precision of LLR is being used to test General Relativity (GR), study the Moon's core, define reference frames, and study geodynamics such as precession and nutation [1, 2, 3]. In particular, GR has come under focus as it is at odds with the other physical understanding of the universe, Quantum Mechanics (QM). QM and GR do not agree on how the universe works at different scales and thus, since QM has been shown to be accurate to extreme precision, the physics community would benefit from gaining more precise measurements of a gravitational system, such as the Earth-Moon system, in order to further test GR and thus validate or refute it in order to unify the physics of different scales.
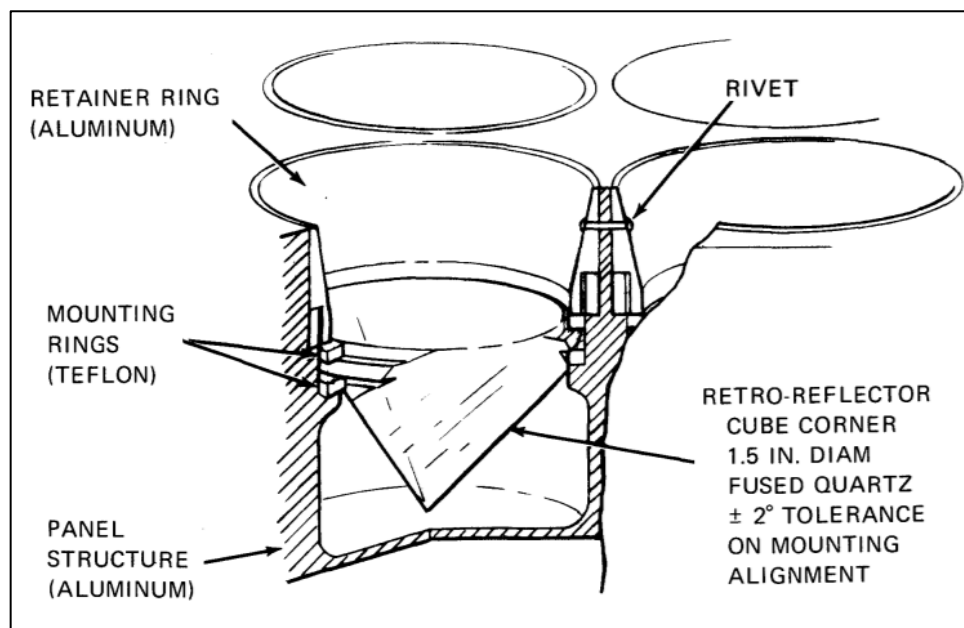
C. Retroreflectors

It is readily apparent that the Moon is visible from Earth and therefore has a reflective surface. The geometric albedo of the Moon, however, is only 12% according to the NASA Space Science Data Coordinated Archive (NSSDCA)[3]. Moreover, the reflected light leaves the Moon at random angles from the terrain, making LLR overly challenging without some way to force the photons to depart the Moon back along the path of arrival. Nonetheless, the first LLR test was conducted by Massachusetts of Technology (MIT) researchers, in the early 1960's, by simply pointing a laser at the natural surface of the Moon [2]. Less than a decade later, Apollo astronauts began deploying retroreflector arrays on the Moon's surface. Retroreflectors are reflective devices with the special property of reflecting light directly back to the source no matter the angle of incidence, via the use of orthogonal surfaces and

---

[3] https://nssdc.gsfc.nasa.gov/planetary/factsheet/moonfact.html

the law of reflection – the incident and reflected angles of a light pulse are equal, and thus two reflections from orthogonal surfaces will reflect the light 180 degrees back in the direction of the light source. In reality, the retroreflectors deployed on the Moon by the Apollo astronauts are limited on exactly how parallel they will reflect the light – beam divergence is the conical expansion of a beam of electromagnetic energy as the distance it travels through space increases. The Apollo retroreflectors impart around 3.75 arcseconds to the beam divergence half-angle of a laser pulse [1]. A mounted lunar retroreflector is shown in Fig. 1 from Alley et al [4] – this is a corner cube type retroreflector, as described next.


Fig. 1 Sketch of a corner cube from an Apollo retroreflector array [4].

There are currently five retroreflector sites on the Moon, distributed as shown in Fig. 2 from Murphy [1]. The Apollo 11, 14, and 15 missions each included the placement of a lunar ranging retroreflector (LRRR) array on the Moon's surface – the reflectors are part of the Lunar Laser Ranging Experiment of the United States of America. The Apollo 11 and 14 arrays each have 100 corner cube type retroreflectors mounted in a metal chassis, while the Apollo 15 array has 300 [5]. The corner cube retroreflectors are made of solid optical glass and are cut to fit into the cylindrical mounts of the chassis. Each corner cube has a reflectivity of 90%, as explored later, and a circular surface diameter of 3.8 cm [5]. The other two retroreflector arrays on the Moon are of French origin, though they were put on the Lunokhod 1 and 2 Soviet lunar rovers, deployed as part of the Luna 17 and 21 missions. The

Lunokhod arrays each have 14 triangular corner cubes with 11 cm edges [1]. A significant difference between the Apollo and Lunokhod corner cubes is that the former use total internal reflection [6], while the latter use silvered rear surfaces [1]. The Lunokhod reflectors are showing signs of degradation (i.e. excessive signal attenuation), likely due to the silvered surfaces [1], and are thus less reliable than the Apollo reflectors. Fig. 3 from Alley et al [4] shows the Apollo 15 retroreflector array.
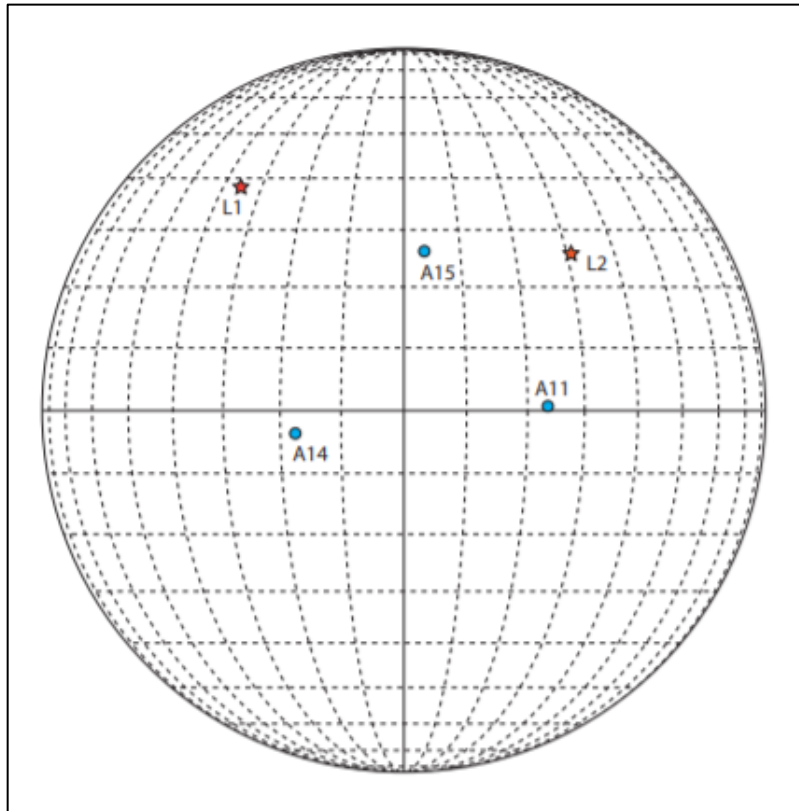
Fig. 2 Distribution of retroreflector sites on the Moon [1].
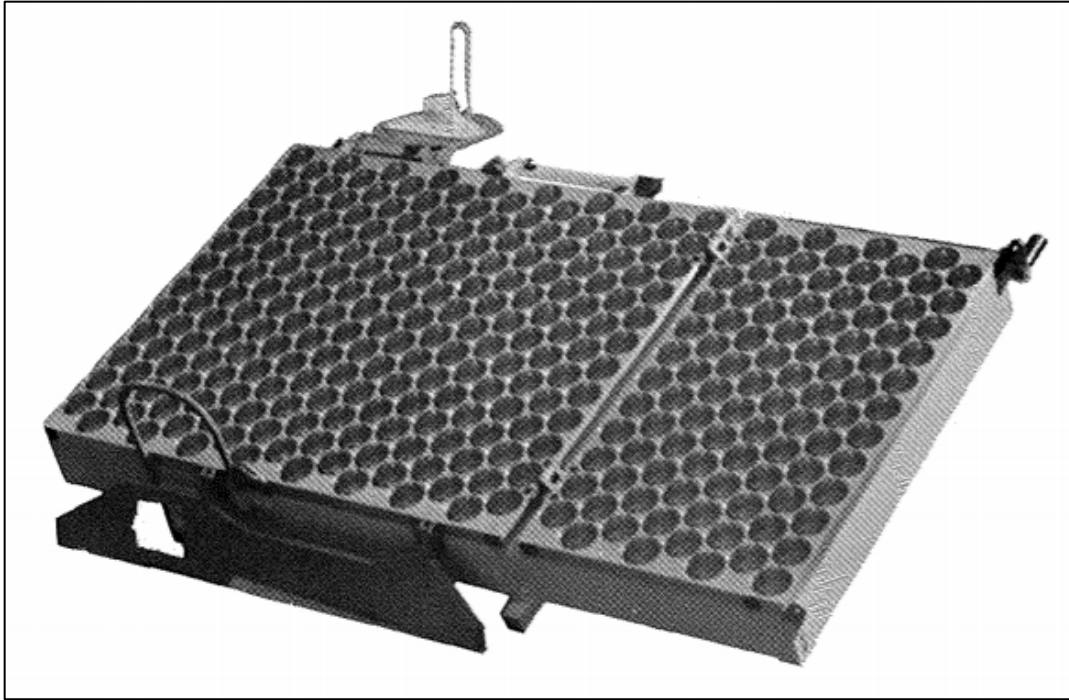
Fig. 3 Apollo 15 retroreflector array with 300 corner cubes [4].

D. Ground Stations

According to the International Laser Ranging Service (ILRS)[4], there are currently three observatories with active lunar laser ranging systems. They are APOLLO at the Apache Point Observatory (observatory code 705) in Sunspot, New Mexico, the McDonald Laser Ranging Station (MLRS) at the McDonald Observatory (observatory code 711) in Fort Davis, Texas, and the MeO station at the Grasse Observatory in Grasse, France operated by the Observatoire de la Cote d'Azur (OCA). Future and former observatories include the Matera Laser Ranging Observatory in Italy, the Geodetic Observatory Wettzell, the Mount Stomlo Satellite Laser Ranging Observatory, the Hartebeesthoek Radio Astronomy Observatory, and the LURE Observatory in Hawaii. As mentioned previously, APOLLO is currently the LLR site with the best performance [1], with a 3 mm measurement RMS (and a total model-based RMS of around 2 cm) due to the ability to collect enough photons per pulse to decrease the uncertainty to that level – the performance of APOLLO will be explored in more detail later.

---

[4] https://ilrs.cddis.eosdis.nasa.gov/index.html

II.   Review of LLR

Before analyzing ground station performance and defining the mission requirements for a satellite LLR system, this section will describe the LLR technique and ground station limitations, as well as some of the benefits of creating an orbiting LLR station.

A. Earth-Moon System

According to Williams et al [7], the range between the laser ranging station and a lunar retroreflector array can be described as the magnitude of the sum of three vectors, as in Eq. (1), where x is the range, r_{EM} is the vector from the center of the Earth to the center of the Moon, r_{RR} is the vector from the center of the Moon to retroreflector array, and r_s is the vector from the center of the Earth to the intersection point of the station optics reference plane and the laser beam axis. The vectors used in Eq. (1) and illustrated in Fig. 4 must be transformed into a common reference frame – typically the Solar System Barycenter (SSB) frame [1]. The presence of multiple retroreflectors on the Moon allows for LLR measurements of more than one site in order to describe the orientation of the Moon and thus determine the appropriate vectors.

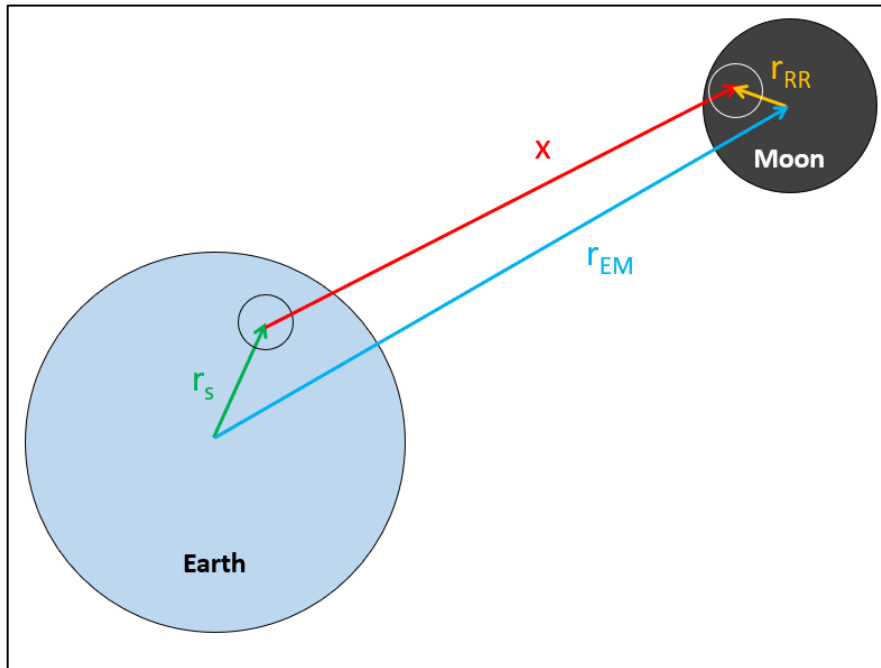$$x = |r_{EM} + r_{RR} - r_s| \tag{1}$$

Fig. 4 Vector map of an LLR station in the Earth-Moon system.

The zenith angle of the laser beam with respect to the Earth can also be used for approximating the distance of the retroreflector array from the center of the Earth. Eq. (2) accomplishes this, where x_E is the distance from the reflector to the center of the Earth and ζ is the zenith angle of the Moon, as seen from the station, with respect to the Earth.

$$x_E = \sqrt{x^2 + |r_s|^2 - 2x|r_s|\cos(\pi - \zeta)} \qquad (2)$$

According to Muller et al. [8], the range to the Moon can also be determined approximately via the average altitude of the Moon above sea-level from Earth, which can be useful for approximating the range used in a preliminary link budget via the link equation presented later. The equation from Degnan [8] is presented here as Eq. (3), where x_m is the mean range, R_E is the mean radius of the Earth, h_s is the altitude of the station above sea-level, and h_M is the mean altitude of the Moon above sea-level.

$$x_m = -(R_E + h_s)\cos\zeta + \sqrt{(R_E + h_s)^2 \cos^2\zeta + 2R_E(h_M - h_s) + h_M^2 - h_s^2} \qquad (3)$$

B. Timing and Atmospheric Delay

The laser ranging technique, as mentioned previously, utilizes the proportionality between the distance light travels and the time it takes the light to travel that distance. Eq. (4) provides this relationship, where x is the distance from the laser source to the ranged target, c is the constant speed of light through vacuum (approximately 299,792 km/s), and Δt_c is the time it takes the light to travel from the source to the target if the entire journey occurs in vacuum. The average pulse TOF for LLR is 2.5 seconds.

$$x = \frac{c}{2}\Delta t_c \qquad (4)$$

The time of flight of the laser pulse is elongated due to atmospheric time delay [2]. This atmospheric effect is due to the index of refraction of the atmosphere being greater than unity – photon propagation speed is slowed down due to molecular interaction with air. Thus, the time of flight of the photons can be more accurately understood via Eq. (5), where Δt_m is the measured time of flight and Δt_{atm} is the random time delay due to travel through the atmosphere.

$$\Delta t_c = \Delta t_m - \Delta t_{atm} \tag{5}$$

As the random time delay due to the atmosphere for any one pulse cannot be exactly known, a model must be employed which invariably imbues the ranging calculation with uncertainty. A great deal of effort by researchers has gone into modeling atmospheric effects in order to account for the complications involving space-pointed ranging through the Earth's atmosphere and to thus enhance the distance measurements between the Earth and Moon to ever increasing precision. Atmospheric effects can cause range inaccuracies of centimeters and even meters [9], but various efforts have been made to correct the ranging values. Atmospheric effects become more noticeable as the observation zenith angle of the moon with respect to the ground station increases, as shown in Fig. 5 taken from Munghemezulu et al [10]. Such observation limitations confine ground-based LLR missions to specific time windows when the Moon is high enough in the sky to allow for suitable measurements.
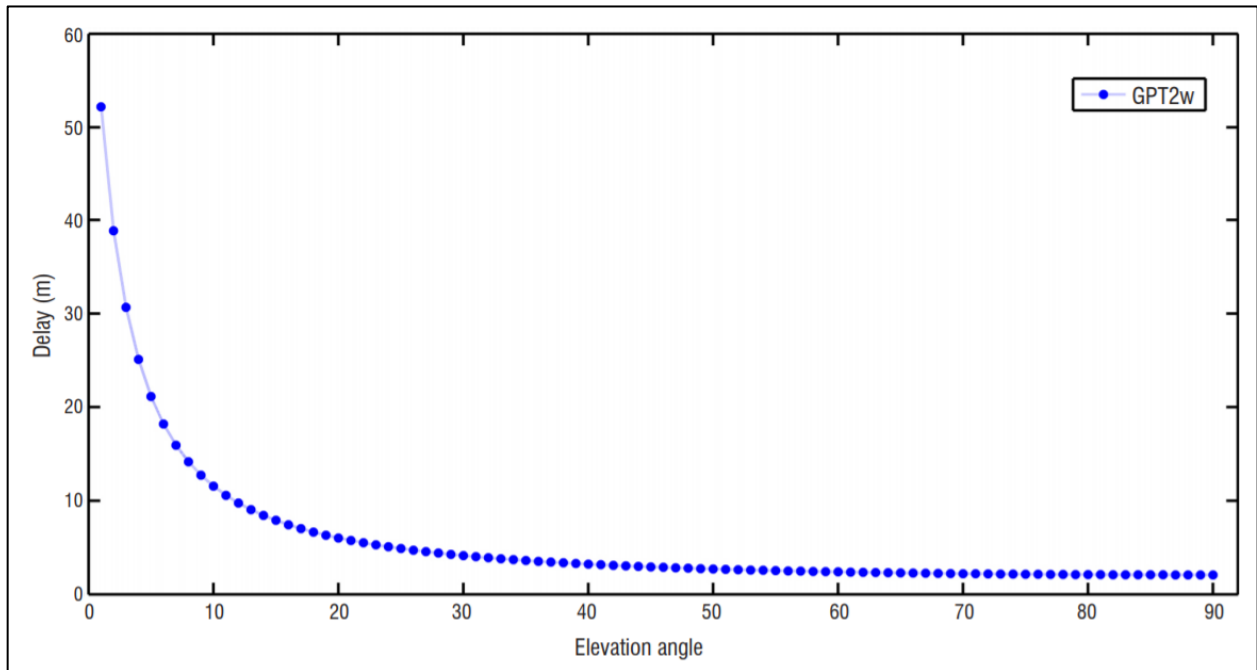
Fig. 5 Computed error in ground-based LLR distance measurements due to elevation angle of the Moon [10].

The OCA [3] and APOLLO [1] stations both employ a calibration reflector, within the observatory, in the path of the LLR pulses for removing clock errors. The calibration reflector has a precisely known distance from the plane of reference of the laser optics, allowing for accurate calibration by geometrically replacing the time of travel between the source and calibration reflector with a precisely known constant time offset. The resulting term in the

equation of Samain et al [3] describing the offset is given here as Eq. (6), where Δt_{calib} is the offset, x_{calib} is the independently measured distance between the source and calibration reflector, and n_{atm} is the index of refraction of the local atmosphere between them. Note that the speed of light divided by the index of refraction is equal to the speed of propagation of the light travelling through the medium having that index of refraction.

$$\Delta t_{calib} = \frac{2}{c/n_{atm}} x_{calib} \tag{6}$$

Eq. (6) can be appropriated for approximately modelling the measured time of flight of the laser light from the source to the Moon, as in Eq. (7), where the index of refraction is a function of altitude, h, and h_s is the altitude of the station. Combining Eqs. (5) and (7) yields Eq. (8), which serves as an approximation of the atmospheric time delay.

$$\Delta t_m = \int_{h_s}^{x+h_s} \frac{2}{c/n_{atm}(h)} dh \tag{7}$$

$$\Delta t_{atm} = \int_{h_s}^{x+h_s} \frac{2}{c/n_{atm}(h)} dh - \Delta t_c \tag{8}$$

The refractive index of the residual atmosphere in LEO was determined in Feng et al [11] to be a function of the surrounding air density when the presence of water is negligible, as given by Eq. (9), where R_{atm} is the specific gas constant (in units of J/kg/K) for dry atmosphere (287.058 J/kg/K) and ρ_{atm} is the atmospheric density (in units of kg/m^3) in the vicinity of the spacecraft.

$$n_{atm} = \frac{6}{773} R_{atm}\rho_{atm} + 1 \tag{9}$$

The MSIS-E-90 Atmospheric Model calculator on NASA's Community Coordinated Modeling Center (CCMC)[5] can be used to approximate the atmospheric total mass density as a function of altitude. Thus, if Eq. (8) and Eq. (9) are combined, the atmospheric time delay is approximated via Eq. (10).

$$\Delta t_{atm} = \int_{h_s}^{x+h_s} \frac{12R_{atm}}{773c} \rho_{atm}(h) dh \tag{10}$$

---

[5] https://ccmc.gsfc.nasa.gov/modelweb/models/msis_vitmo.php

For a LEO orbit at 500 km above sea-level, the MSIS model outputs a local atmospheric total mass density on the order of 10^{-13} kg/m^3. For a finite step increase of 1 m in altitude from the orbit, the increase in timing delay would be on the order of 10^{-9} picoseconds, or an increase in the measured range on the order of tenths of picometers for a difference on the order of 10^{-5} m/s in light propagation speed from the absolute value in vacuum – as the light travels toward the Moon, the index of refraction would decrease even more drastically. This result seems to be in agreement with the assertion in Davis et al [12] that atmospheric delays are significant at altitudes up to the troposphere and mesosphere layers of the atmosphere – an altitude of 500 km is well into the thermosphere, which is above the troposphere and mesosphere. Thus, the atmosphere for a satellite in a LEO orbit at 500 km above sea-level is not expected to induce significant photon delay during an LLR mission, regardless of non-negligible drag – in other words, Δt_m in Eq. (7) reduces to Δt_c as Δt_{atm} approaches zero (for a negligible ρ_{atm} with respect to laser ranging).

C. Atmospheric Photon Loss

In addition to causing time delays, the atmosphere can also cause loss of the ranging photons. This loss can be accounted for via electromagnetic absorption by the atmosphere, as well as atmospheric scattering of the photons. Fig. 6 from Fingas et al [13] shows the effect of absorption and scattering on the transmission of various wavelengths of light through the atmosphere – visible light is attenuated by fifty to sixty percent. The loss of photons further decreases the certainty in the ranging measurements due to each laser pulse having a finite temporal width. Important to note is that the atmosphere also increases the divergence of an outbound laser pulse [1] due to atmospheric turbulence [8], as discussed later. The combination of atmospheric time delay, atmospheric photon loss, and increased divergence makes the Earth's atmosphere nonoptimal for visible light LLR. A significant benefit of conducting LLR via orbiting satellites is thus the ability to remove the entire system from the challenges associated with the atmosphere.
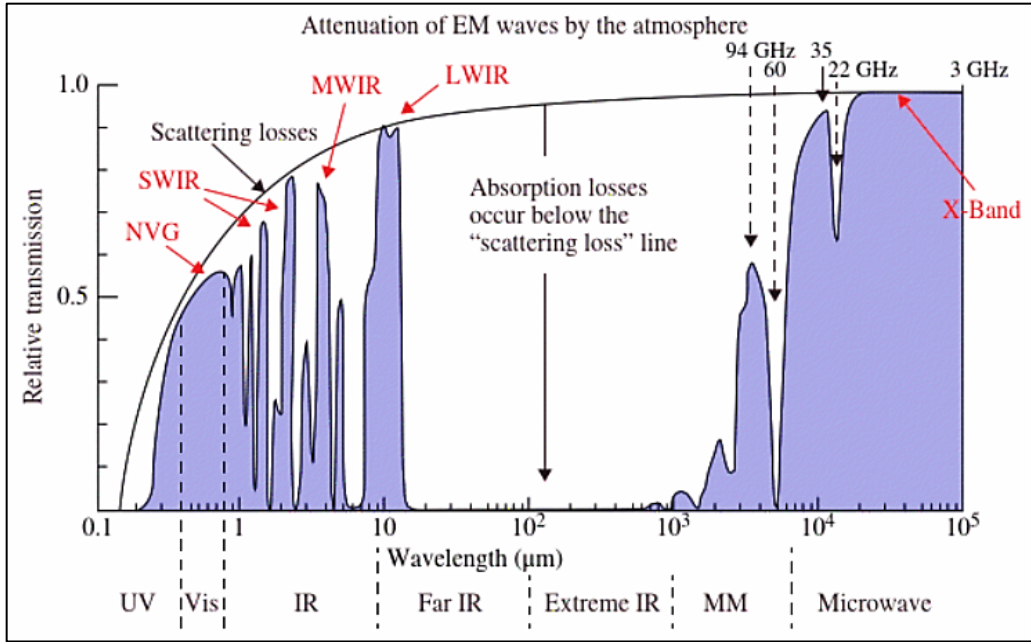
Fig. 6 Atmospheric transmission spectrum of ultra-violet to microwave wavelengths [13].

D. Ground Dynamics

According to Miller et al [14], tidal effects can displace ground stations by multiple centimeters. Fig. 7 from Munghemezulu et al [10] shows simulation results for ground station vertical displacement due to tides over the course of one month, depicting an elevation displacement range of 55 cm. Modeling ground dynamics, such as tidal displacement, is used for approximating actual elevation of LLR ground stations for purposes of increasing the accuracy of ranging calculations. Other effects on ground elevation include atmospheric and oceanic pressure loading. The necessity of taking ground dynamics into consideration for LLR could be eliminated by implementing an on-orbit LLR system instead of relying on a ground-based LLR system, although the effects of atmospheric drag and solar radiation on the orbiting system should be explored. An LLR mission in LEO utilizing GPS positioning for the mission spacecraft could provide an independent measurement source for the lunar distance that could be used for comparison with ground-based LLR systems.
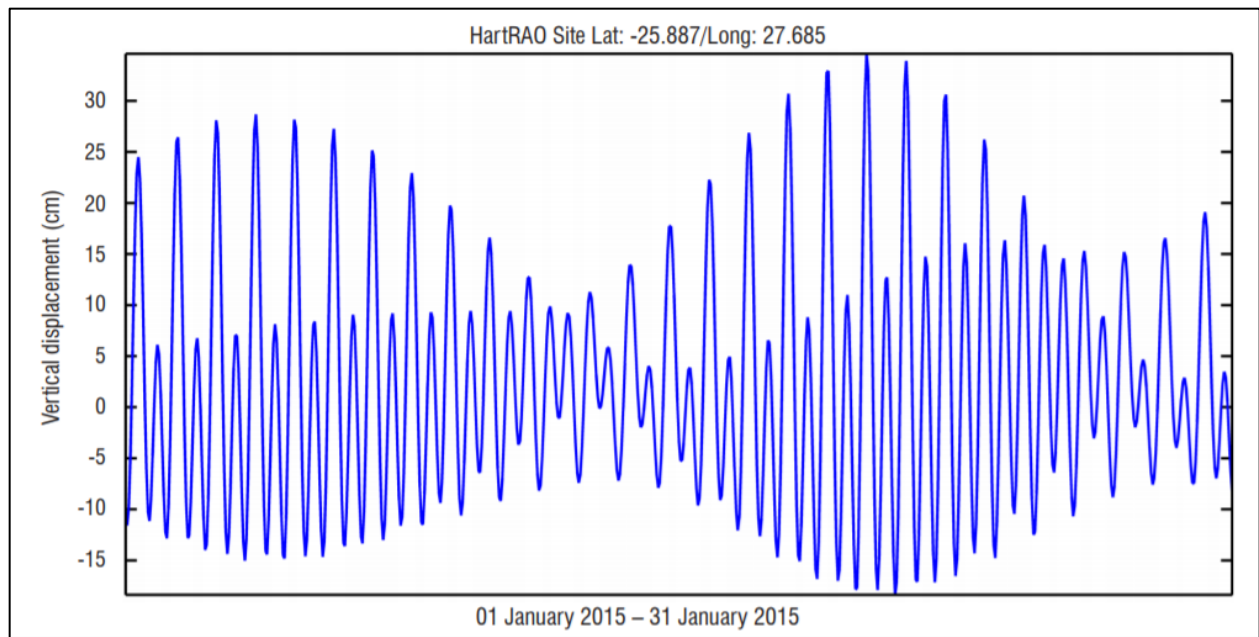
Fig. 7 Simulation of vertical displacement of a ground station due to tidal effects [10].


E. LRRR Wavelength Compatibility

As mentioned previously, the Apollo corner cubes do not use reflective coatings and rely on total internal reflection because aluminizing the back surfaces of the glass would cause heating from solar radiation, which could degrade the surfaces and thus diminish their utility for precision LLR. Similarly, the corner cubes are made of fused silica due to the material being transparent to most of the solar radiation spectrum [15] – fused silica demonstrates excellent transmission of approximately 90% for wavelengths of 250 nm to 2000 nm, as shown in Fig. 8 taken from Ledemi et al [16], while solar radiation has non-zero spectral irradiance starting at wavelengths above 250 nm, peaking between 500 nm and 750 nm before greatly reducing past 2000 nm, as shown in Fig. 9 taken from Bozzetti et al [17]. Thus, any laser wavelength between 250 nm and 2000 nm should be sufficient for LLR pointed at the Apollo LRRR sites, but atmospheric absorption and scattering have confined ground-based LLR to visible wavelengths and the infrared "transmission windows" [13], precluding the use of much of the ultraviolet wavelength range – refer back to Fig. 6. An LLR system in LEO would not need to account for measurement degradations due to atmospheric absorption and scattering, thus allowing for the use of UV wavelengths, as well as IR wavelengths outside of the transmission windows that confine ground-based measurements to only pockets of the full IR range,

so long as the chosen wavelengths are within the fused silica compatibility range of transmission. Advancements in

IR lasers in the 1.5 μm wavelength range make them attractive for an orbiting LLR system.
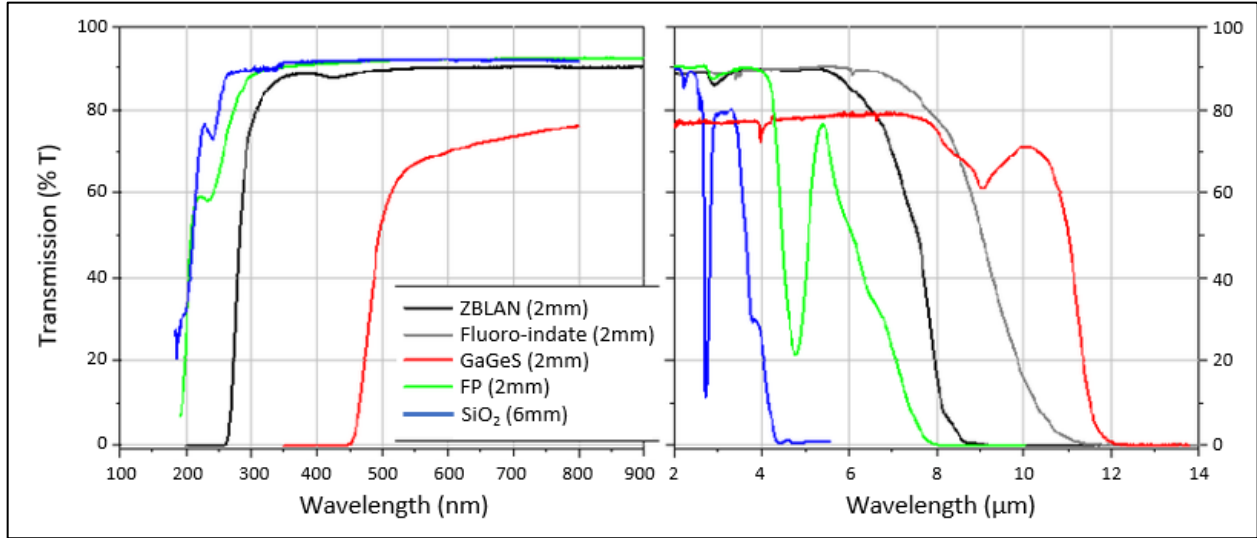
Fig. 8 Transmission of photons through glass (the blue line is the transmission spectrum of fused silica) [16].
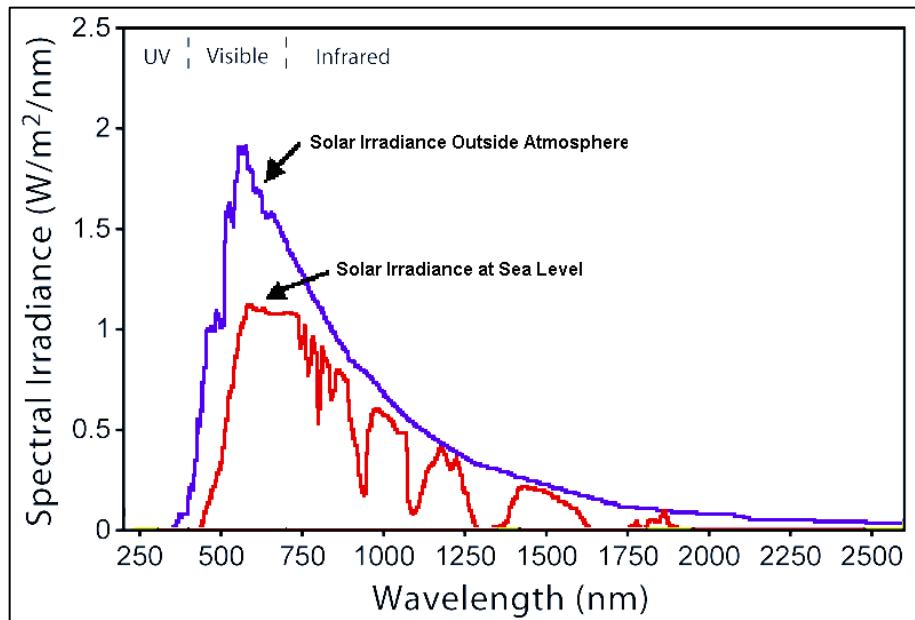
Fig. 9 Solar radiation spectrum (the blue line is the solar radiation spectrum in near-Earth space) [17].

F. Detector Efficiency

During the first decade of the LLR experiment, ruby lasers were utilized with a red 694 nm wavelength. The LLR system operated by OCA in Grasse, France used a 694 nm ruby laser from 1970 to 1986 before switching to an Nd:YAG laser at an infrared 1064 nm wavelength – second harmonic generation is utilized in order to produce a green 532 nm wavelength [18]. The switch from red to green photons was made due to the higher quantum efficiency of the green photon detectors at the time [18]. The quantum efficiency for various types of photon detectors has increased for green and non-green wavelengths alike, meaning they can now be used more effectively for LLR. One type of photon detector is a charge-coupled device (CCD) that senses the charge generated by the incident photons on the surface in order to detect them. As an example, the CCD's utilized by the Transiting Exoplanet Survery Satellite (TESS) exhibit quantum efficiencies of over 90% for wavelengths in the range of 600 nm to 900 nm before dropping off to less than 30% quantum efficiency at 1000 nm, as shown in Fig. 10 taken from Krishnamurthy [19]. Other photon detector types include avalanche photon detectors (APD's), which can have efficiencies above 90% as well, including for infrared (IR) wavelengths, and photomultiplier tubes (PMT's). Thus, the wavelength of the laser pulse used for LLR from LEO should be selected for compatibility with the transmission spectrum of the fused silica corner reflectors in conjunction with the use of a photon detector with a sufficient quantum or collection efficiency for that wavelength. It is important to note that detector efficiency and laser wavelength directly affect the photon ratio of the link budget presented in the next section.
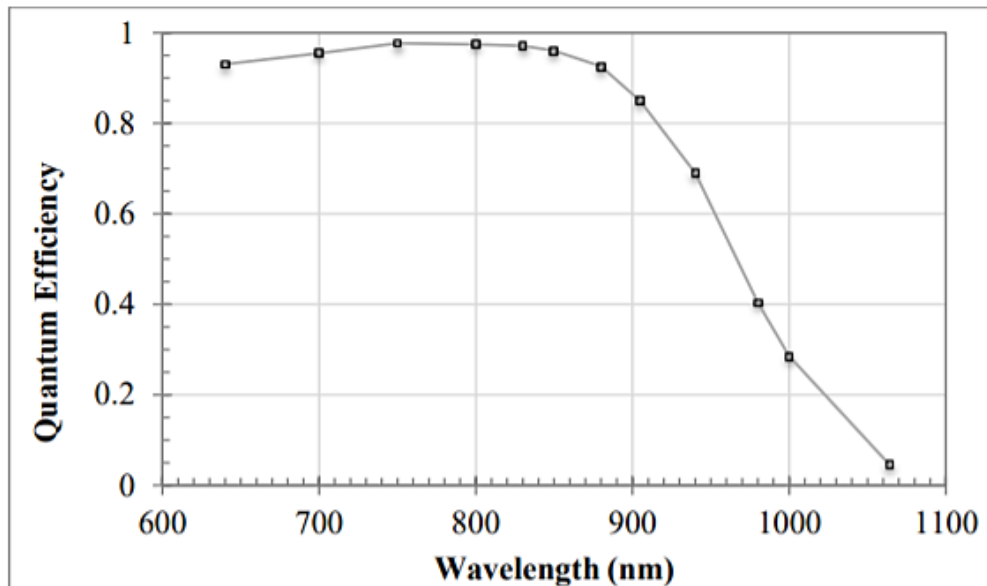

Fig. 10   Quantum efficiency of the TESS CCD's [19].

III. Radiometry Review

In this section, Gaussian beams will be explained and the link budget for an LLR mission will be derived. An example pointing requirement will then be provided and the performance of the APOLLO station with be reviewed, with comparison to the expected results of the link equation. The mission requirements for a LEO LLR system will then be explored in the section following this one.

A. Gaussian Beams and Pointing

A Gaussian beam is an idealized model of the distribution of photons radially from the center axis of the laser beam where the distribution is a Gaussian distribution. The edge of a Gaussian beam is defined to be at the radial distance, from the center axis of the beam, where the intensity falls off to I_{max}/e^2, correlating to a radial distance of two standard deviations (2σ), where I_{max} is the peak intensity of the laser beam, located at the center axis.

According to Thomas et al [20], the quality of a laser beam, M^2, according to ISO standard 11146, can be defined as the ratio of the laser's beam parameter product to the diffraction limited Gaussian beam parameter product for the wavelength of the laser. The beam parameter product of a laser is the product of θ, the beam divergence half-angle of the laser, and w_0, the beam waist radius of the laser. The diffraction limited beam parameter product is the wavelength, λ, divided by π. Eq. (11) illustrates this definition of beam quality. A diffraction limited laser beam therefore has an M^2 value of exactly one and θ is inversely proportional to w_0 with a constant of proportionality equal to λ/π, as in Eq. (12).

$$M^2 = \frac{\theta w_0}{\lambda/\pi} \tag{11}$$

$$\theta = \frac{\lambda}{\pi w_0} \tag{12}$$

The beam divergence causes the beam to expand radially as it travels through space. The radius, w_f, of a Gaussian beam at some distance, x, in the far field can be approximated using Eq. (13). The spot area of the beam at x can then be determined as in Eq. (14) for a circular beam cross section. Fig. 11 illustrates the divergence of a Gaussian beam for far field approximations. For a range much greater that the beam waist radius, which is the case
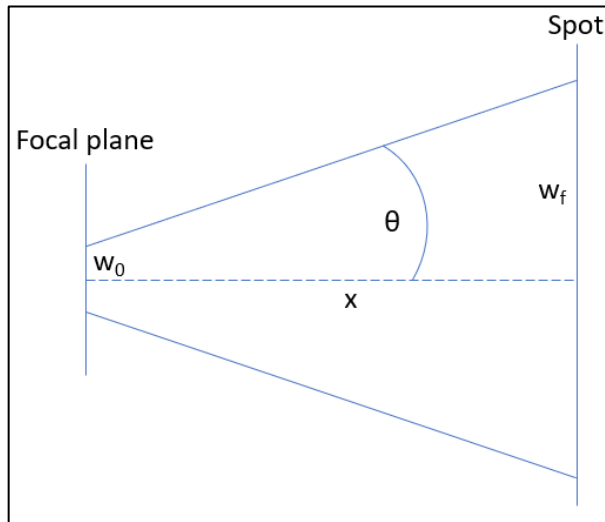
for LLR in the far field, the w_0 term in Eq. (13) can be neglected. As implied previously, the radial standard deviation of the Gaussian beam is half of the far field radius, as expressed in Eq. (15). The maximum intensity of a Gaussian beam is determined via Eq. (16), where P_{TX} is the output power of the laser.

$$w_f = w_0 + x \tan \theta \tag{13}$$

$$A_f = \pi w_f^2 \tag{14}$$

$$\sigma = \frac{w_f}{2} \tag{15}$$

$$I_{max} = \frac{2P_{TX}}{\pi w_f^2} \tag{16}$$

Fig. 11   Gaussian beam divergence for the far field.

As mentioned previously, the retroreflectors on the Moon also impart some degree of divergence on a laser pulse. For a range much greater than the size of the retroreflector array, this again being the case for LLR in the far field, the spot area at the receiver of the reflected pulse, assuming it is at the same position as the transmitter, is given by Eq. (17), where A_s is the spot area at the station and γ is the divergence half-angle imparted by the retroreflectors. According to Murphy [1], the divergence half-angle of the lunar retroreflectors is approximately 3.75 arcseconds.

$$A_s = \pi x^2 \tan^2(\theta + \gamma) \tag{17}$$

For a ground station, the minimum distance from the station to the lunar surface can be approximated as the Moon's perigee minus the mean radii of the Earth and Moon, or approximately 355,200 km. At such a position, the Moon would have an angular size of 33.6 arcminutes from the perspective of the station. If the Gaussian laser beam on the station exits the Earth's atmosphere with a beam divergence half-angle of 20 arcseconds, the beam would have a spot diameter twice the value of w_f found via Eq. (13), or approximately 68.9 km, corresponding to roughly 2% of the Moon's diameter. A pointing error angle of 20 arcseconds would thus bring the edge of the Gaussian beam to the reflector, whereupon the intensity of the photons incident on the reflector array would decrease to $1/e^2$ of the maximum. Thus, as a fundamental limit, the pointing error angle should be kept less than the beam divergence half-angle. At that limit, the 20 arcsecond pointing error angle would lead to a transverse pointing error distance equal to w_f, radially outward from the beam's center axis. Thus, the center axis of the beam should not be farther than 34.4 km from the reflector array at the lunar surface.

The actual pointing requirement is constrained by the desired photon ratio in the link budget equation, presented as Eqs. (33) through (35). If the requirement is stated as maintaining the center axis of the beam pointed at an angle, relative to the line joining the station and reflector, at which the photons incident on the reflector have an intensity greater than or equal to the intensity of the beam at a radial distance 1σ away from the center axis, then the maximum transverse pointing error distance of the center axis from the line, via Eq. (15), would be one fourth of the lunar spot diameter, or approximately 17.2 km, correlating to a maximum pointing error angle of 10.0 arcseconds, via Eq. (18), where φ_{TX} is the pointing error of the laser.

$$\max(\varphi_{TX}) = \operatorname{atan}\left(\frac{\sigma}{x}\right) = \operatorname{atan}\left(\frac{1}{2}\tan\theta\right) \tag{18}$$

According to Wang et al [21], piezoelectric fast steering mirrors can be implemented as actuators in a feedback control system for fast tracking applications. In this mission, pointing error angle could be fed into the control loop for minimization during LLR activities in order to maximize the intensity of the return signal on the photon detector, which would increase the number of photons received per pulse for measurement, as explored in the next subsection of this paper. Fig. 12 illustrates such a control loop. Pointing vectors can be estimated via the use of star trackers and inertial measurement sensors.
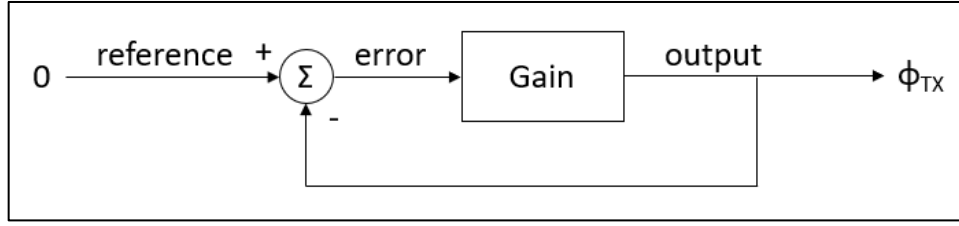
Fig. 12 Control loop for minimizing φ$_{TX}$.

B. Link Budget

Of utmost importance in any electromagnetic ranging application is the ratio of the number of photons received to the number of photons launched by the transmitter. Various effects will cause the loss of a large number of the launched photons, leading to only a small number of photons returning for TOF measurements. The photon ratio is described via the link equation. Eq. (19) is the link equation for this mission design, with respect to the formulations of Degnan [8] and Marshall et al [22], and with the added effect of thermal degradation of the central irradiance of the corner cube reflectors, as noted in Murphy [1], here implemented as a unique efficiency, ε_{RR}. In Eq. (19), n_{RX} is the number of photons observed by the receiver, n_{TX} is the total number of photons in the laser pulse sent out by the transmitter, η_q is the quantum efficiency of the photon detector, η_{TX} is the efficiency of the transmitting optics, η_{RX} is the efficiency of the receiver optics, ρ_{RR} is the reflectivity of the corner cubes, N_{RR} is the number of corner cubes in the LRRR array, G_{TX} is the transmitter gain, G_{RR} is the corner cube gain, G_{RX} is the receiver gain, F_{TX} is the free space path loss from the transmitter, F_{RR} is the free space path loss from the reflector, L_{TX} is the transmitted pointing loss factor [23], L_{RR} is the reflected pointing loss factor, T_{atm} is the transmissivity of the atmosphere, and T_{cirrus} is the transmissivity of encountered cirrus clouds. An additional efficiency parameter, η_{NL}, is added to account for non-linear effects and other effects that are not otherwise accounted for. The number of photons in a laser pulse can be determined via Eq. (20), where h is Planck's constant ($6.62607004/10^{34}$ m^{2}kg/s) and E_{TX} is the energy of the pulse. In turn, the energy of the pulse is determined, via Eq. (21), where f_p is the pulse rate of the laser.

$$\frac{n_{RX}}{n_{TX}} = \eta_{NL}\eta_q(\eta GFL)_{TX}(\rho N\varepsilon GFL)_{RR}(\eta G)_{RX}(T_{atm}T_{cirrus})^2 \tag{19}$$

$$n_{TX} = \frac{\lambda}{hc}E_{TX} \tag{20}$$

$$E_{TX} = \frac{P_{TX}}{f_p} \tag{21}$$

The effective area, A_{eff}, is characteristic of a specific wavelength and is given by Eq. (22). The area of the reflector, A_{RR}, and area of the receiver, A_{RX}, are given by Eqs. (23) and (24), respectively, where D_{RR} is the diameter of one of the corner cubes and D_{RX} is the diameter of the receiver optics. The three gains, G_{TX}, G_{RR}, and G_{RX}, are determined from the formulations of Degnan [8] and Marshall et al [22], expanded into their intrinsic components. G_{TX} is given by Eq. (25) where it is evident that it depends only on the beam divergence half-angle (including any contributions in divergence half-angle by atmospheric turbulence [8], θ_{atm}). G_{RR} is given by Eq. (26) as the square of the ratio of A_{RR} to A_{eff} and depends only on the corner cube diameter and wavelength. G_{RX} is given by Eq. (27) as the ratio of A_{RX} to A_{eff} and depends only on receiver optical diameter and wavelength.

$$A_{eff} = \frac{\lambda^2}{4\pi} \tag{22}$$

$$A_{RR} = \frac{\pi}{4}D_{RR}^2 \tag{23}$$

$$A_{RX} = \frac{\pi}{4}D_{RX}^2 \tag{24}$$

$$G_{TX} = \frac{8}{(\theta+\theta_{atm})^2} \tag{25}$$

$$G_{RR} = \left(\frac{A_{RR}}{A_{eff}}\right)^2 = \left(\frac{\pi D_{RR}}{\lambda}\right)^4 \tag{26}$$

$$G_{RX} = \frac{A_{RX}}{A_{eff}} = \left(\frac{\pi D_{RX}}{\lambda}\right)^2 \tag{27}$$

F_{TX} is the free space path loss from the station to the LRRR, as given by Eq. (28), while F_{RR} is the free space path loss from the LRRR back to the station. The free space path losses depend only on their associated ranges and on the wavelength. For the LLR application, F_{TX} and F_{RR} happen to be the same.

$$F_{TX} = F_{RR} = \frac{A_{eff}}{4\pi x^2} = \left(\frac{\lambda}{4\pi x}\right)^2 \tag{28}$$

Note that G_{TX} can be derived via Eq. (29) where I_{max} for the Gaussian beam is determined via Eq. (16), after

inserting Eq. (13) with the tangent of the divergence half-angle approximately equal to the divergence half-angle

itself for small angles and with w_0 much smaller than w_f. The result, after simplifying the expression and

incorporating the added divergence imparted by the atmosphere, is Eq. (25).

$$G_{TX} = \frac{I_{max}}{F_{TX}\frac{P_{TX}}{A_{eff}}} \tag{29}$$

For a Gaussian beam, the transmitter pointing loss factor [23], L_{TX}, of the transmitted Gaussian beam due to

pointing error and with respect to the transmitter gain formulation of Degnan [8] is given by Eq. (30). Such a

pointing loss factor accounts for the decrease in intensity the farther off-axis the photons that hit the reflector are

from the center axis of the laser pulse. There is also a pointing loss factor caused by the station being rotated off-axis

from the laser beam center axis during the TOF of the laser pulse. This is defined as a pointing loss factor associated

with the retroreflectors, L_{RR}, and takes into account both the beam divergence and the divergence imparted by the

retroreflectors themselves, discussed previously. The resulting reflected pointing loss factor is given by Eq. (31).

Note that both Eqs. (30) and (31) incorporate the effect of atmospheric divergence.

$$L_{TX} = \exp\left(-2\left[\frac{\varphi_{TX}}{\theta+\theta_{atm}}\right]^2\right) \tag{30}$$

$$L_{RR} = \exp\left(-2\left[\frac{\varphi_{RR}}{\theta+\theta_{atm}+\gamma}\right]^2\right) \tag{31}$$

Combining Eqs. (19) through (21), (25) through (28), (30), and (31), the resulting link budget, where Eq. (32)

has been utilized for the sake of space (μ here is considered as the overall efficiency of the system), is given by Eq.

(33), which is then expanded into Eq. (34) by replacing θ via Eq. (12). It is evident that the number of photons

observed by the photon detector depends on which LRRR is targeted (i.e. N_{RR}), the power and pulse rate of the laser,

the wavelength, the size of the transmitter (i.e. w_0), the size of the receiver, the lunar ranges, and the pointing error

angles, as well as the overall efficiency of the system. Note that T_{atm} and T_{cirrus} are taken to be unity for the LEO

LLR mission (and θ_{atm} is taken to be zero), as previously explored, and that M^2 is assumed to be unity (i.e. the laser

beam is diffraction limited). For an LLR system of a leader and follower satellite with no relative distance error

during pulse interception by the follower (referred to as perfect satellite orbital phasing in this paper), Eq. (34) reduces to Eq. (35).

$$\mu = \eta_{NL}\eta_q\eta_{TX}\eta_{RX}\varepsilon_{RR}\rho_{RR}(T_{atm}T_{cirrus})^2 \tag{32}$$

$$n_{RX} = \frac{\mu N_{RR}P_{TX}D_{RR}^4}{32hcf_p\lambda}\left(\frac{\pi D_{RX}}{(\theta+\theta_{atm})x^2}\right)^2 e^{-2\left(\left[\frac{\varphi_{TX}}{\theta+\theta_{atm}}\right]^2+\left[\frac{\varphi_{RR}}{\theta+\theta_{atm}+\gamma}\right]^2\right)} \tag{33}$$

$$n_{RX} = \frac{\mu N_{RR}P_{TX}(\pi D_{RR})^4}{32hcf_p\lambda}\left(\frac{w_0 D_{RX}}{(\lambda+\pi w_0\theta_{atm})x^2}\right)^2 e^{-2\pi^2 w_0^2\left(\left[\frac{\varphi_{TX}}{\lambda+\pi w_0\theta_{atm}}\right]^2+\left[\frac{\varphi_{RR}}{\lambda+\pi w_0(\theta_{atm}+\gamma)}\right]^2\right)} \tag{34}$$

$$n_{RX} = \frac{\mu N_{RR}P_{TX}}{32hcf_p\lambda^3}\left(\frac{\pi D_{RR}\sqrt{w_0 D_{RX}}}{x}\right)^4 e^{-2\left[\frac{\pi w_0\varphi_{TX}}{\lambda}\right]^2} \tag{35}$$

C. APOLLO Performance

APOLLO currently has the best performance of the operating LLR stations, with a photon ratio on the order of 10^{-18} to 10^{-17}, aperture diameter of 3.5 m, pulse rate of 20 Hz, average power of 2.3 W, and diffraction limited beam divergence half-angle of 0.02 arcseconds at a wavelength of 532 nm, though the atmosphere typically induces an added beam divergence half-angle of around 0.5 arcseconds [1]. For the 3.75 arcsecond divergence half-angle imparted by the Apollo corner cubes and the effective beam divergence half-angle of 0.52 arcseconds, the divergence half-angle of the reflected photons from the retroreflector array is 4.27 arcseconds. For a 1σ equivalent maximum pointing error, the maximum pointing error angle, φ_{TX}, via Eq. (18), is 0.26 arcseconds. The intensity at the 1σ radial distance from the center axis of the beam is 60.65% of maximum, via Eq. (30).

Making a grand simplification by assuming APOLLO is at the equator of the Earth and that the orbit of the Moon has no inclination with respect to the equator of the Earth, and assuming a range equal to the mean distance of the Moon from the Earth (here taken to be the Moon's orbital semi-major axis of 384,400 km, according to the NSSDCA), the station would have rotated away from the center axis of the beam by 37.66 arcseconds due to the rotation of the Earth. This would correspond to a pointing error angle, φ_{RR}, of the return pulse from the reflector back to the station of approximately 0.64 arcseconds, via the law of cosines, using an altitude for the station of 2.8 km above sea-level [1]. Thus, the intensity of the return pulse would be 95.64% of the return pulse maximum, via

Eq. (31). The total decrease in intensity due to divergence and pointing error is then the product of Eqs. (30) and (31), resulting in a total decrease of 41.99% from the maximum intensity of the outbound pulse.

Using the link budget of Eq. (33) – taking into account the 15% of maximum central irradiance of the corner cubes [1, 24] and their 90% reflectivity (refer back to Fig. 8) and the 30% quantum efficiency of the APOLLO avalanche photodiode (APD) array used as a photon detector [1], and assuming 50% efficiency of the transmitting and receiving optics and 50% transmission through the atmosphere (refer back to Fig. 6) and cirrus clouds, as well as an η_{NL} of 50% to account for non-linear effects (e.g. frequency doubling of the Nd:YAG laser from 1064 nm to 532 nm) – the number of photons estimated to be received by the station is calculated to be 1.24 photons per pulse for the Apollo 11 and 14 arrays (with an N_{RR} of 100) and 3.71 for the Apollo 15 array (with an N_{RR} of 300). This approximately agrees with the statistics reported for APOLLO of 1.52 photons per pulse for the Apollo 14 array and 3.15 photons per pulse for the Apollo 15 array [1].

IV.   LEO Mission Design

The mission concept presented in this paper is to place an LLR station in orbit around the Earth, particularly in Low Earth Orbit (LEO). The objective is to have an LLR station that is independent from ground measurements and the uncertainties associated with space-pointing ground-based observations (e.g. atmospheric delays and vertical ground displacement). To achieve an orbiting LLR capability, the system presented utilizes a formation of two satellites, where the leader carries the transmitter equipment and the follower carries the receiver equipment. The leader fires the laser at the Moon and the follower intercepts the laser pulse as it returns from the Moon, while both satellites are orbiting around the Earth at high speeds. GPS will be used for position data of the satellites instead of satellite laser ranging (SLR) in order to avoid complicating the system with the ground-based uncertainties, needing dedicated SLR station access, and limiting the LLR time windows. Thus, the positioning data accuracy attainable from the GPS and the timing synchronization of the multiple satellites is important. This mission would also require an attitude control system that can support the pointing requirements of the laser, plus inter-satellite distance control sufficient for the follower satellites in the formation to maintain sufficient capability to receive the reflected photons while in orbit. Fig. 13 illustrates the mission concept. Ranging to multiple reflector arrays, distributed on the lunar surface, in a short time span allows for determination of the Moon's orientation, used for vector determinations.
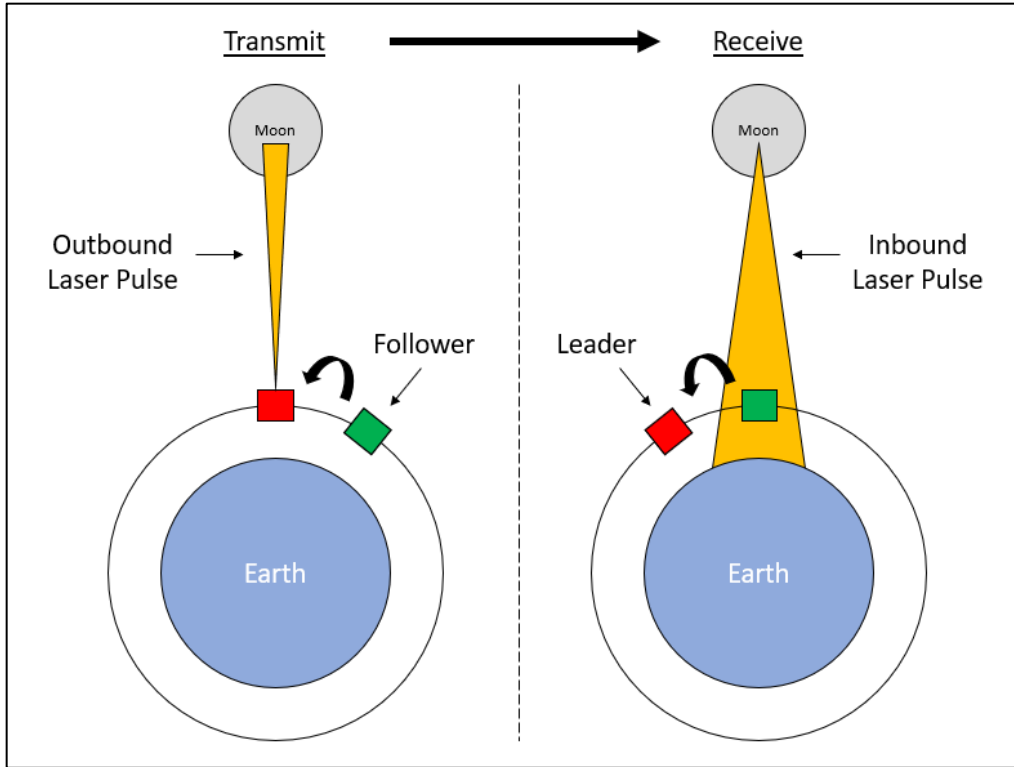
Fig. 13   Illustration of LEO LLR leader-follower satellite formation concept.

D. Satellite Formation Positioning

The mission utilizes GPS for positioning of the satellites in their orbits at various times. Helleputte et al [25] suggests centimeter level accuracy for GPS positioning, while Bertiger et al [26] suggests the possibility of sub-centimeter level accuracy. The leader-follower intersatellite separation distance could potentially also be obtained via separate intersatellite ranging systems (e.g. another laser on the leader in conjunction with retroreflectors on the follower for intersatellite ranging [27], or even an S-band frequency radar system [28]) for increased accuracy. A chip scale atomic clock (CSAC) can be used on-board each of the LEO satellites with sufficient radiation resistance, possibly an SA.45s CSAC by Microsemi after sufficient testing, as mentioned later. The Time Transfer by Laser Experiment (T2L2) on the Jason 2 satellite demonstrated an uncertainty of less than 140 picoseconds for synchronization of remote clocks [29]. Quantum computing techniques could also possibly be used for precision synchronization of the multiple orbiting platforms involved in the measurements.

E. Satellite Formation Separation

If the orbital plane of the satellite formation is in the orbital plane of the Moon and the orbit of the satellite formation is circular, then the minimum distance, x_{min}, between the leader and the lunar surface is when the Moon is at perigee in its orbit and the leader is at a point on the line joining the center of the Earth to the center of the Moon. The maximum distance, x_{max}, considering a symmetric LLR measurement window about that line, would be the range of the satellite at the beginning or end of that window when the Moon is at apogee in its orbit – refer to Fig. 14. The resulting expressions for x_{min} and x_{max} are Eq. (36) and (37), respectively, where h_{cs} is the altitude above sea-level of the satellites in their circular orbit, r_{Mp} and r_{Ma} are the distances (363,300 km and 405,500 km, respectively, according to the NSSDCA) from the center of the Earth to the center of the Moon when the Moon is at perigee and apogee, respectively, R_E is the mean radius of the Earth (6371 km, according to the NSSDCA), and R_M is the mean radius of the Moon (1737.4 km, according to the NSSDCA). The window half-angle, A, determines x_{max}. The sum of h_{cs} and R_E is here defined to be r_{cs}.

$$x_{min} = r_{Mp} - r_{cs} - R_M \qquad (36)$$

$$x_{max} = \sqrt{r_{cs}^2 + r_{Ma}^2 - 2r_{cs}r_{Ma}\cos A} \qquad (37)$$
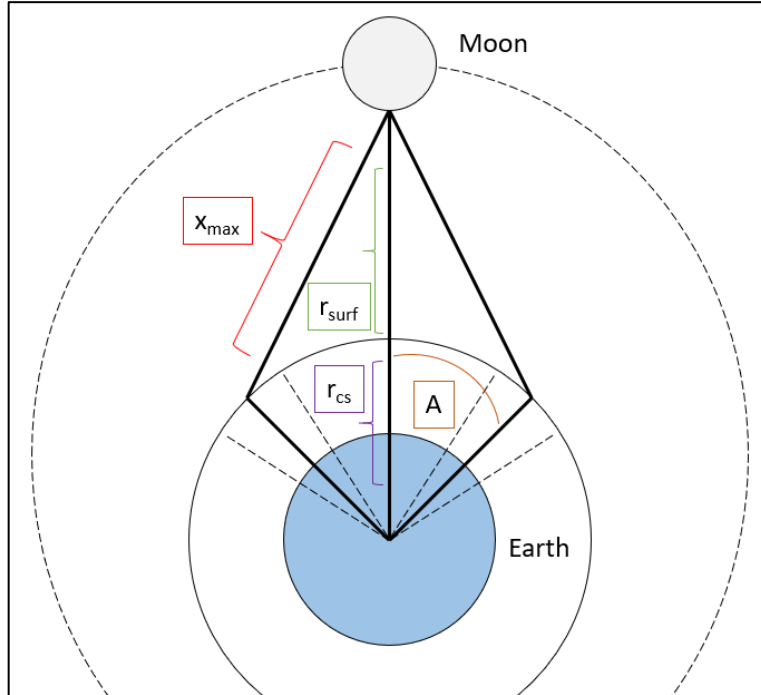
Fig. 14   Geometry of ranging window at max range, with the Moon is at apogee, assuming a symmetric window; here, r_{surf} is the distance from the satellite to the surface of the moon at 0 degree off-center, r_{cs} is the distance from the center of the Earth to the satellite orbit, and A is the maximum off-center angle of the leader satellite (the angle off-center at which the measurement window begins and ends).

For the circular orbit, the necessary arc length, S, between the two satellites in order for the follower satellite to intercept the return photons at the position where the leader fired the laser is the product of the TOF and the tangential velocity, v_{cs} given by Eq. (38), of the circular orbit, where μ_E is the gravitational parameter of the Earth (398,600 km^3/m^2). The expression for S is given in Eq. (39). Recognizing that the length of a circular arc is the product of its radius of curvature and the angle between its endpoints, the chord distance, d, between the two satellites separated by S is given by Eq. (40). Therefore, the minimum and maximum necessary linear distances, d_{min} and d_{max}, respectively, between the leader satellite and follower satellite are given by Eqs. (41) and (42), respectively, as functions of h_{cs}, by incorporating Eqs. (36) and (37), respectively, within Eq. (39) and combining with Eq. (40).

$$v_{cs} = \sqrt{\frac{\mu_E}{h_{cs}+R_E}} \tag{38}$$

$$S = \frac{2}{c} x_1 \sqrt{\frac{\mu_E}{h_{cs}+R_E}} \tag{39}$$

$$d = (h_{cs} + R_E)\sqrt{2\left[1 - \cos\left(\frac{S}{h_{cs}+R_E}\right)\right]} \tag{40}$$

$$d_{min}(h_{cs}) = (h_{cs} + R_E)\left(2\left[1 - \cos\left(\frac{2}{c}\frac{(\mu_E)^{\frac{1}{2}}}{(h_{cs}+R_E)^{\frac{3}{2}}}\left[r_{M_p} - h_{cs} - R_E - R_M\right]\right)\right]\right)^{\frac{1}{2}} \tag{41}$$

$$d_{max}(h_{cs}) = (h_{cs} + R_E)\left(2\left[1 - \cos\left(\frac{2}{c}\frac{(\mu_E)^{\frac{1}{2}}}{(h_{cs}+R_E)^{\frac{3}{2}}}\left[\sqrt{r_{cs}^2 + r_{Ma}^2 - 2r_{cs}r_{Ma}\cos A}\right]\right)\right]\right)^{\frac{1}{2}} \tag{42}$$

For an h_{cs} of 500 km, Eq. (41) gives a d_{min} of 47.3 km and Eq. (42) gives a d_{max} of 61.1 km. Thus, for this h_{cs}, the follower satellite will need to be 47.3 km away from the leader when the leader fires the laser, if the Moon is at perigee, and 61.1 km from the leader satellite if the Moon is at apogee, in order to intercept the return pulse, on average, 2.5 seconds later – the minimum TOF, found via Eq. (4), of the laser pulse for the x_{min} of 354,700 km,

found via Eq. (36), is 2.37 seconds, while the maximum TOF for the x_{max} of 407,400 km, found via Eq. (37), is 2.69 seconds. The precision required for the intersatellite distance is anlayzed in the next subsection.

Specialized orbits could also be explored, such as orbits where the Moon is always out of Earth's shadow, which would allow for continuous LLR at any time. Highly eccentric orbits could also be explored where LLR would be conducted at apogee to take advantage of the decreased dynamics. Cold gas thrusters or rotating panels for differential drag control could be used for satellite formation maintenance and modification of intersatellite distance for photon ratio maximization (i.e. minimization of intercept position error, explored next, and thus minimization of φ_{RR}).

F. Mission Requirements

The LEO LLR preliminary system design, using infrared, is presented here, along with an ultraviolet alternative at lower power, for an altitude of 500 km above sea-level. The low power ultraviolet alternative is designed in such a way as to have the same performance as the APOLLO station, namely the same photons per pulse received for measurement on the photon detector. For performance analysis, the system is assumed to have perfect satellite phasing for the follower satellite considered (i.e. no relative positioning error, though relative positioning error will be explored for the uncertainty requirements) and the performance values are described here for the follower satellite.

The infrared laser in this preliminary design is an Er:Yb type operating at a 1535 nm wavelength. The power is increased from the 2.3 W of APOLLO to 25 kW, while the pulse rate is kept the same as APOLLO at 20 Hz, producing 1.25 kJ pulses that are 100 ps in temporal width. Thus, more photons are contained in each transmitted pulse, namely 9,660 quintillion instead of 308 quadrillion.

A main advantage of the LEO LLR system is that it is removed from the atmosphere. This offers several benefits, including the absence of the divergence imparted by the atmosphere and the absence of atmospheric and ice crystal absorption and scattering. Thus, T_{atm} and T_{cirrus} are set at unity and the divergence is only dependent on the laser size and wavelength, not the atmosphere. The 1535 nm (and 355 nm, for the low-power ultraviolet alternative system) wavelength is possible because the atmosphere is not present to block specific infrared wavelengths (nor the ultraviolet wavelengths) from being used for LLR, which is otherwise supported by the transmission compatibility of the fused silica corner cubes of the Apollo arrays.

An array of avalanche photodiodes (APD's) could be used as the photon detector on the receiver. Voxtel sells laser-ranging InGaAs APD's with wide spectral response, compatible with wavelengths between 950 nm to 1700 nm and with a collection efficiency of upwards of 90%[6]. The Grasse LLR station in France was recently upgraded with an InGaAs APD module for photon detection [18]. Thus, the photon detector will be switched from the 30% collection efficiency APD system of APOLLO to a 90% collection efficiency APD system. The other efficiency values are kept the same as in the previous performance analysis of the APOLLO station, namely η_{NL}, η_{TX}, and η_{RX} at 50% each, and with ε_{RR} at 15% [1, 24]. The altitude of the station is of course increased from 2.8 km to 500 km. The transmitter and receiver diameter are reduced from the 3.5 m aperture of APOLLO to 10 cm each, an order of magnitude smaller, leading to a photon detection per pulse an order of magnitude higher than APOLLO, namely 12.75 photons per pulse for the Apollo 14 array, instead of 1.52, and 38.26 photons per pulse for the Apollo 15 array, instead of 3.15. Tables 1 and 2 tabulate the design specifications and performance values. The small size for the transmitter and receiver, 10 cm in diameter, makes the mission feasible, as compared to needing to send multiple 3.5 m apertures into orbit. If the aperture diameter is increased above 10 cm, then the number of photons detected per pulse will also increase.

Table 1 System design of LEO LLR system compared to APOLLO (with system parameter values from Murphy [1])

	APOLLO (Murphy [1])	Ultraviolet Alternative	LEO IR LLR Design
Laser Type	Nd:YAG	Nd:YAG	Er:Yb
Laser Mode	Frequency Doubled	Frequency Tripled	N/A
Wavelength	532 nm	354.67 nm	1535 nm
Power	2.3 W	2.3 W	25 kW
Pulse Rate	20 Hz	20 Hz	20 Hz
Pulse Energy	115 mJ	115 mJ	1.25 kJ
Photons/Pulse	308×10^{15}	205×10^{15}	9.66×10^{21}
Pulse Width	100 ps	100 ps	100 ps
Transmitter Diameter	350 cm	19 cm	10 cm
Receiver Diameter	350 cm	19 cm	10 cm
Quantum Efficiency	30%	90%	90%

Table 2 Performance of LEO LLR system compared to APOLLO (with performance data from Murphy [1])

Quantity	Array	Origin	APOLLO	Ultraviolet	LEO IR LLR

[6] https://voxtel-inc.com/products/photoreceivers-ingaas

				Alternative	Design
Photons/Pulse	Apollo 14	Measured	1.52 (Murphy [1])	-	-
Photons/Pulse	Apollo 14	Budget	1.24	1.25	12.75
Photon Ratio	Apollo 14	Measured	4.9×10^{-18}	-	-
Photon Ratio	Apollo 14	Budget	4.0×10^{-18}	6.0×10^{-18}	1.32×10^{-21}
Photons/Pulse	Apollo 15	Measured	3.15 (Murphy [1])	-	-
Photons/Pulse	Apollo 15	Budget	3.71	3.72	38.26
Photon Ratio	Apollo 15	Measured	1.0×10^{-17}	-	-
Photon Ratio	Apollo 15	Budget	1.2×10^{-17}	1.8×10^{-17}	3.96×10^{-21}

The results also verify that S1 would not be able to detect any photons on its own. The beam divergence half-angle leaving the reflector is 5.77 arcseconds and thus the pointing error angle, φ_{RR}, for a satellite at the Gaussian edge of the return beam would be 2.88 arcseconds. For the leader satellite, φ_{RR} would be 10.48 arcseconds, and thus more than 1.8 times removed from even the edge of the return pulse, assuming a Gaussian distribution. This indicates the necessity for the two satellite formation, as opposed to a single satellite conducting an LLR mission on its own.

The APOLLO station operates a 2.3 W laser with a 532 nm wavelength at a pulse repetition rate of 20 Hz, which creates a series of 115 mJ pulses for approximately 1 hour of LLR, on average, 260 nights per year [1] – this is due to both time allocation and elevation suitability of the Moon in the sky to minimize atmospheric effects. Each pulse has a temporal width of 100 ps, which is the maximum recommended due to the orientation and finite size of the retro reflectors – they cause a temporal spread of between 200 and 300 ps, and thus the pulse width should be no more than 100 ps to prevent negatively impacting the error budget [1]. The 20 Hz pulse rate helps maintain a suitable signal-to-background ratio (SBR). Increasing the pulse rate frequency negatively effects the SBR - doubling the repetition rate would cut the SBR in half when using a 1 ns temporal filter [1]. Thus, the 20 Hz rate will be maintained for this mission based on the experience of the APOLLO station.

The RANGE CubeSat was designed with a 25 kW laser from Voxtel operating at a 1535 nm wavelength, but has a pulse width of 4 ns – thus, it does not meet the pulse width requirement of 100 ps. The beam divergence is 2.5 degrees, which, assuming a diffraction limited beam, gives a beam waist radius of 11.2 μm. Thus, the exact system design used for RANGE is not suitable for this mission. Instead, custom optics could be used with a transmit and receive diameter of 10 cm, for compatibility with the CubeSat form factor, and with a 1535 nm wavelength, leading to a diffraction limited beam divergence half-angle of 2.02 arcseconds. In order to maintain an intensity on the retroreflector of at least the intensity located one standard deviation away from the center axis (where the peak

intensity of the beam is located) the pointing requirement will be the ability for the laser beam to maintain a pointing error angle of less than 1.01 arcsecond, meaning that, in reality, sub-arcsecond pointing is required. APOLLO targets multiple reflector sites in a circuit during its measurement activities, which allows for describing the orientation of the Moon [1], necessary for determining the vectors used for calculating the center-to-center distance of the Earth and Moon. It is therefore a requirement for the satellite system to do so, as well.

The temporal spread of the photons due to the difference in position of the multiple corner cubes in an array can approach 1 ns at full-width-at-half-maximum (FWHM), or an RMS, σ_0 in Eq. (43), exceeding 300 ps [1]. A 1 mm scaled RMS, σ_d in Eq. (44), translates to a 6.67 ps detection timing resolution requirement, σ_t in Eqs. (43) and (44) – the relative timing synchronization requirement for the mission is thus a precision below 10 ps, which also implies a frequency stability on the order of 10^{-12} during a period of a few seconds [1] (the CSAC's from Microsemi[7] have a stability less than 10^{-11}, and thus would need to be tested to ensure that they are suitable for the mission). Thus, for scaling by the square root of the number of photons detected, 1 mm precision can be statistically attained with around 2000 photons, N. For the mission system design described, using a 100 corner cube array as an example, the number of photons detected per pulse, per the link budget, is estimated to be 12.75 at a circularized altitude of 500 km above sea-level. Thus, 150 pulses would be required over a time-span of 7.5 seconds at the 20 Hz repetition rate. APOLLO would take 65 seconds to collect 2000 photons from 1,300 pulses at 20 Hz, for the maximum observed 1.52 photons per pulse.

$$\sigma_d = \frac{c}{2}\sigma_t \tag{43}$$

$$N = \left(\frac{\sigma_0}{\sigma_t}\right)^2 \tag{44}$$

APOLLO LLR measurements carry a predicted uncertainty of less than 3 mm, RMS. However, the LLR data must be combined with a model in order to account for displacement effects and other error effects. The Jet Propulsion Laboratory (JPL) model is currently the best model available and is the used on the APOLLO data, giving an RMS of around 2 cm. Of those 2 cm, 3 mm are due to the actual measurement RMS, but up to 5 mm of RMS are due to ocean loading and 1 mm of RMS is added for every 3 mbar of atmospheric pressure loading [1]. Thus, for preliminary mission design, the measurement RMS for the LEO LLR system is designed to simply be less

---

[7] https://www.microsemi.com/product-directory/embedded-clocks-frequency-references/5207-space-csac

than 2 cm, due to the absence of ground-based uncertainties. Solar radiation pressure and atmospheric drag in LEO could present their own effects on measurement uncertainty and should thus be explored in future analyses. First and foremost, the absolute position of the leader satellite when it fires the laser should be known to an accuracy of less than 2 cm. This is not an unreasonable task for modern GPS. The relative time, however, with regards to photon detection, must be accurate to a few picoseconds, as discussed, which is achievable with modern timing electronics combined with an effective photon detector. The absolute time and, subsequently, the relative position uncertainty of the satellites to one another must also be understood, as is explored next.

For this preliminary design, the satellite orbit and orbit of the Moon around the Earth are assumed to be coplanar. The APOLLO station collects around 1 hour of measurements per day for 260 days per year, or around 260 hours of data per year [1]. The circularized altitude of the satellites is set at 500 km above sea-level. At this altitude, the satellites have an orbital rate of 1.1 mrad/s around the Earth, or an orbital period of around 94.47 minutes - they would orbit the Earth 15.24 times per day. Thus, in order to collect 1 hour of measurements per day, the LEO LLR system would need to collect measurements for 236.17 seconds per orbit. Thus, the satellites would move in their orbit by around 15 degrees during each measurement window – the measurement window half-angle, A, in Eq. (37) and Fig. 14, is thus 7.5 degrees. This translates to around a 4.17% duty cycle per orbit for the LLR system.

If the leader satellite begins each measurement window at 7.5 degrees off from the line joining the center of the Moon to the center of the Earth, as illustrated in Fig. 14, the measurement error will be minimized, as opposed to taking measurements farther off-center. At 7.5 degrees off-center, the maximum range between the pulse launch point and the surface of the Moon (when the Moon is at apogee) would be 354,751 km, as opposed to the 354,691 km at 0 degrees off-center. The range measurement would vary by less than 2 cm if the relative intersatellite position is off-target by 10 cm, translating to an absolute timing requirement of 10 ms. When the Moon is at perigee, the follower satellite, at the beginning of the window, if at the maximum 10 cm offset from target position, would induce 14 mm RMS if trailing the target position or 3 mm RMS if flown past it; this is vice-versa at the end of the window. For the Moon at apogee, the 10 cm relative position requirement would lead to an RMS range between 5 mm and 14 mm instead. This confirms that the calculated range distance would have an RMS of less than 2 cm. As calculated previously, the minimum and maximum separation distances of the leader and follower satellite within the measurement window are 47.3 km and 61.1 km, respectively. Thus, when the Moon is at perigee, the minimum follower distance from the leader should be 47.3 km +/- 10 cm, while, when the Moon is at apogee, the maximum

follower distance from the leader should be 61.1 km +/- 10 cm, in order to intercept the return pulse at the appropriate times for range calculations that are accurate to less than 2 cm. The mission requirements are summarized in Table 3, in which it appears that achieving the minimum mission requirements is a feasible task with modern technologies.

Table 3 Summary of Mission Requirements

Maximum Pulse Width	100 ps
Pulse Repetition Rate	20 Hz
Maximum Transmit-Receive Diameter	10 cm
Maximum Pointing Error Angle	1 arcsecond
Relative Timing Accuracy	~ 7 ps
CSAC Frequency Stability @ < 10 seconds	~ 10^{-12}
Absolute Timing Accuracy	< 10 ms
Relative Positioning Accuracy @ < 100 km	< 10 cm
Absolute Positioning Accuracy	< 2 cm
Minimum Mission Duration	260 days
Minimum Laser Duty Cycle	4%

V.   Conclusion

LLR has always been a ground-based science. Over the decades since the Lunar Laser Ranging Experiment began, LLR science has contributed to the understanding of physics, the Earth and Moon, and laser technology. LLR stations have gradually become more accurate in their ability to measure the Earth-Moon distance. However, they have been plagued by the atmosphere and ground movement. By establishing an LLR station in orbit around the Earth, the challenging effects of both the atmosphere and the ground could be avoided. Link budgeting shows that such an LLR station in LEO is feasible with an aperture size an order of magnitude smaller than the aperture of the APOLLO station, a size which can be accommodated on small satellites. A satellite formation conducting LLR in LEO could offer an independent measurement source to verify the results of the measurements of the ground stations and potentially enhance the accuracy of the measurements by avoiding the use of atmospheric and ground dynamic models. The LEO LLR station could potentially detect more photons per pulse than APOLLO and the range determination accuracy of the APOLLO station, after input into the JPL LLR model, seems to be attainable by the LEO LLR system. The topic of LLR in LEO seems to be worth further exploration as it appears to be feasible

and could offer a new perspective to the science of LLR with the potential to enhance the understanding of the Earth-Moon system and the physical laws that govern it.

References

[1] Murphy, T. W., Jr., "Lunar Laser Ranging: The Millimeter Challenge," *Reports on Progress in Physics*, Vol. 76, No. 7, 14 June 2013.

doi: 10.1088/0034-4885/76/7/076901

[2] Williams, J. G., Turyshev, S. G., and Boggs, D. H., "Lunar Laser Ranging Tests of the Equivalence Principle with the Earth and Moon," *International Journal of Modern Physics D*, Vol. 18, No. 7, 2 Jan. 2009, pp. 1129–1175.

doi: 10.1142/S021827180901500X

[3] Samain, E., Mangin, J. F., Veillet, C., Torre, J. M., Fridelance, P., Chabaudie, J. E., Feraudy, D., Glentzlin, M., Pham Van, J., Furia, M., Journet, A., and Vigouroux, G., "Millimetric Lunar Laser Ranging at OCA (Observatoire de la Cote d'Azur)," *Astronomy and Astrophysics Supplement Series*, Vol. 130, No. 2, 15 June 1998, pp. 235–244.

doi: 10.1051/aas:1998227

[4] Alley, C. O., Bender, P. L., Currie, D. G., Dicke, R. H., Faller, J. E., Kaula, W. M., MacDonald, G. J. F., Mulholland, J. D., Plotkin, H. H., and Wilkinson, D. T., "Lunar Ranging Retro-Reflector (LRRR) Familiarization Manual (Revision A)," NAS 9-5829, Lunar Surface Project Office, Manned Spacecraft Center, Aerospace Systems Division, The Bendix Corporation, 1 May 1971.

[5] Dickey, J. O., Bender, P.L., Faller, J. E., Newhall, X. X., Ricklefs, R. L., Ries, J. G., Shelus, P. J., Veillet, C., Whipple, A. L., Wiant, J. R., Williams, J. G., and Yoder, C. F., "Lunar Laser Ranging: A Continuing Legacy of the Apollo Program," *Science*, Vol. 265, No. 5171, 22 July 1994, pp. 482–490.

doi: 10.1126/science.265.5171.482

[6] Turyshev, S. G., Williams, J. G., Folkner, W. M., Gutt, G. M., Baran, R. T., Hein, R. C., and Somawardhana, R. P., "Corner-cube retro-reflector instrument for advanced lunar laser ranging", *Experimental Astronomy*, Vol. 36, No. 1-2, Aug. 2013, pp. 105-135.

doi: 10.1007/s10686-012-9324-z

[7] Muller, J., Williams, J. G., and Turyshev, S. G., "Lunar Laser Ranging Contributions to Relativity and Geodesy," *Lasers, Clocks, and Drag-Free Contro*l, edited by Dittus, H., Lammerzahl, C., and Turyshev, S. G., Astrophysics and Space Science Library Book Series, Springer, Berlin, Vol 349, 2008, pp. 357–372.

doi: 10.1007/978-3-540-34377-6_21

[8] Degnan, J. J., "Millimeter Accuracy Satellite Laser Ranging: A Review," *Contributions of Space Geodesy to Geodynamics: Technology*, edited by Smith, D. E. and Turcotte, D. L., Geodynamics Series Book Series, American Geophysical Union, Washington, DC, Vol. 25, 1 Jan. 1993, pp. 1593–1607.

doi: 10.1029/GD025p0133

[9] Currie, D. G., and Prochazka, I., "Atmospheric Effects and the Ultimate Ranging Accuracy for Lunar Laser Ranging (3055)," NASA, International Laser Ranging Service, Nineteenth International Workshop on Laser Ranging, Session 13: Lunar Laser Ranging, Annapolis, 27-31 Oct. 2014.

[10] Munghemezulu, C., Combrinch, L., and Botai, J. O., "A review of the lunar laser ranging technique and contribution of timing systems," *South African Journal of Science*, Vol. 112, No. 3-4, 2016.

doi: 10.17159/sajs.2016/20150400

[11] Feng, D. D., and Herman, B. M., "Remotely Sensing the Earth's Atmosphere Using the Global Positioning System (GPS) – The GPS/MET Data Analysis," *Journal of Atmospheric and Oceanic Technology*, Vol. 16, 1 Aug. 1999, pp. 989–1002.

doi: 10.1175/1520-0426(1999)016<0989:RSTESA>2.0.CO;2

[12] Davis, J. L., Herring, T. A., Shapiro, I. I., Rogers, A. E. E., and Elgered, G., "Geodesy by radio interferometry: Effects of atmospheric modeling errors on estimates of baseline length," *Radio Science*, Vol. 20, No. 6, Nov.–Dec. 1985, pp. 1593–1607.

doi: 10.1029/RS020i006p01593

[13] Fingas, M., and Brown, C. E., "Oil Spill Remote Sensing," *Handbook of Oil Spill Science and Technology*, edited by Fingas, M., John Wiley & Sons, Inc., Hoboken, 2015, Chap. 12, pp. 313-356.

[14] Muller, J., and Tesmer, V., "Investigation of tidal effects in lunar laser ranging," *Journal of Geodesy*, Vol. 76, No. 4, Apr. 2002, pp. 232-237.

doi: 10.1007/s00190-001-0239-0

[15] Faller, J. E., "Laser Ranging Retro-Reflector Experiment," NAS 9-11025, Physics Dept., Wesleyan Univ., Middleton, CT, Sept. 1973.

[16] Ledemi, Y., El-Amraoui, M., Calvez, L., Zhang, X. H., Bureau, B., and Messaddeq, Y., "Colorless chalco-halide Ga2S3-GeS2-CsCl glasses as new optical material", *Photonic Fiber and Crystal Devices: Advances in Materials and Innovations in Device Applications VII*, 884704, Vol. 8847, SPIE, San Diego, 2013.

doi: 10.1117/12.2024461

[17] Bozzetti, M., de Candia, G., Gallo, M., Losito, O., Mescia, L., and Prudenzano, F., "Analysis and Design of a Solar Rectenna," *2010 IEEE International Symposium on Industrial Electronics*, 11653438, IEEE, Bari, 4-7 July 2010.

doi: 10.1109/ISIE.2010.5637486

[18]   Courde, C., Torre, J. M., Samain, E., Martinot-Lagarde, G., Aimar, M., Albanese, D., Exertier, P., Fienga, A., Mariey, H., Metris, G., Viot, H., and Viswanathan, V., "Lunar laser ranging in infrared at the Grasse laser station," *Astronomy & Astrophysics*, Vol. 602, No. A90, 21 June 2017.

doi: 10.1051/0004-6361/201628590

[19]   Krishnamurthy, A., Villasenor, J., Thayer, C., Kissel, S., Ricker, G., Seager, S., Lyle, R., Deline, A., Morgan, E., Sauerwein, T., and Vanderspek, R., "Quantum efficiency measurement of the Transiting Exoplanet Survery Satellite (TESS) CCD detectors", *Space Telescopes and Instrumentation 2016: Optical, Infrared, and Millimeter Wave*, 99042W, Vol. 9904, SPIE, Edinburgh, 2016.

doi: 10.1117/12.2232244

[20]   Thomas, N., Spohn, T., Barriot, J. P., Benz, W., Beutler, G., Christensen, U., Dehant, V., Fallnich, C., Giardini, D., Groussin, O., Gunderson, K., Hauber, E., Hilchenbach, M., Iess, L., Lamy, P., Lara, L. M., Lognonne, P., Lopez-Moreno, J. J., Michaelis, H., Oberst, J., Resendes, D., Reynaud, J. L., Rodrigo, R., Sasaki, S., Seiferlin, K., Wieczorek, M., and Whitby, J., "The BepiColombo Laser Altimeter (BELA): Concept and baseline design," *Planetary and Space Science*, Vol. 55, No. 10, July 2007, pp. 1398–1413.

doi: 10.1016/j.pss.2007.03.003

[21]   Wang, G., and Rao, C., "Adaptive control of piezoelectric fast steering mirror for high precision tracking application," *Smart Materials and Structures*, Vol. 24, No. 3, 10 Feb. 2015.

doi: 10.1088/0964-1726/24/3/035019

[22]   Marshall, W. K., and Burk, B. D., "Received Optical Power Calculations for Optical Communications Link Performance Analysis," NASA N87-15329 07-32, Nov. 1986, pp. 32-40.

[23]   Rathore, S., and Rathore, D., "Effect of Transmitter Pointing Error Angle on InterSatellite Communication," *International Journal of Current Engineering and Technology*, Vol. 5, No. 3, June 2015, pp. 1939–1941.

[24]   Goodrow, S. D., and Murphy, T. W., Jr., "Effects of thermal gradients on total internal reflection corner cubes," *Applied Optics*, Vol. 51, No. 36, 2012, pp. 8793-8799.

doi: 10.1364/AO.51.008793

[25]   Helleputte, T. V., Doornbos, E., and Visser, P., "CHAMP and GRACE accelerometer calibration by GPS-based orbit determination," *Advances in Space Research*, Vol. 43, No. 12, June 2009, pp. 1890–1896.

doi: 10.1016/j.asr.2009.02.017

[26]   Bertiger, W., Desai, S. D., Dorsey, A., Haines, B. J., Harvey, N., Kuang, D., Sibthorpe, A., and Weiss, J. P., "Sub-Centimeter Precision Orbit Determination with GPS for Ocean Altimetry," *Marine Geodesy*, Vol. 33, No. Sup 1, 9 Aug. 2010, pp. 363–378.

doi: 10.1080/01490419.2010.487800

[27]   Gao, P., and You. Z., "Characters and development of laser ranging technology on small-satellite relative position measurement," *Second International Conference on Space Information Technology*, 67952G, Vol. 6795, SPIE, Wuhan, 2007.

doi: 10.1117/12.774803

[28]   Alawieh, M., Hadaschik, N., Franke, N., and Mutschler, C., "Inter-Satellite Ranging in the Low Earth Orbit," *2016 10th International Symposium on Communication Systems*, Networks and Digital Signal Processing (CSNDSP), 16336655, IEEE, Prague, 20-22 July 2016.

doi: 10.1109/CSNDSP.2016.7573920

[29]   Samain, E., Exertier, P., Courde, C., Fridelance, P., Guillemot, P., Laas-Bourez, M., and Torre, J.-M., "Time transfer by laser link: a complete analysis of the uncertainty budget," *Metrologia*, Vol. 52, No. 2, 1 Apr. 2015, pp. 423-432.

doi: 10.1088/0026-1394/52/2/423